Inverted Pendulum Report

James Teng, Ethan Ng, Tuong Bao Nguyen

1 Introduction

The primary objective is to design and implement a feedback control system to balance an inverted pendulum mounted on a LEGO MINDSTORM EV3 robot, maintaining the upright position in the presence of external disturbances. This serves as a practical application of model based design, spanning system identification, controller synthesis, and hardware validation. Key equipment include:

LEGO EV3 Robot A two wheeled platform with a motor driven pendulum assembly mounted at the front, capable of independent motion control for both wheel movement and pendulum actuation.

MATLAB and Simulink Used for both controller simulation and "External Simulation", where computer code is compiled and executed directly on the LEGO robot hardware, enabling closed-loop controller design, simulation, and real time deployment.

Sensors A gyroscope mounted on the pendulum provides angular rate measurements for feedback, while motor encoders supply wheel position data to support the concurrent drive system from Workshop 3.

These tools bridge the gap between theoretical modeling and physical implementation, enabling evaluation of the closed-loop control system against specifications for phase margin, disturbance rejection, and complimentary sensitivity bandwidth.

2 System Modeling

2.1 Model Derivation

The system can be modelled by a non-linear system by forming a sum of rotational torques. By equating the pendulum's moment of inertia multiplied by its angular acceleration to the three components of its motion (gravity, frictional force, and a motor torque dictated by a voltage input), we can derive a differential equation in terms of angular position (θ) and input voltage (v):

$$\ddot{\theta}(t) + b\dot{\theta}(t) - ksin(\theta(t)) - cv(t) = 0$$

This can be converted to a linear approximation of the system given a sufficiently small input, resulting in the plant function:

$$\frac{\Delta_\theta(s)}{\Delta_v(s)} = \frac{c}{s^2 + bs + k}$$

2.2 Model Parameters

To determine the parameters of the system, the pendulum was flipped in order to ensure the system was stable, and a pulse was input into the arm of the pendulum. The resulting oscillation was recorded, and used to calculate each value.

Equating the above transfer function to the second order canonical function allows us to approximate the system plant function:

$$\frac{c}{s^2 + bs + k} = \frac{c}{s^2 + 2\zeta\omega_n s + \omega_n^2}$$

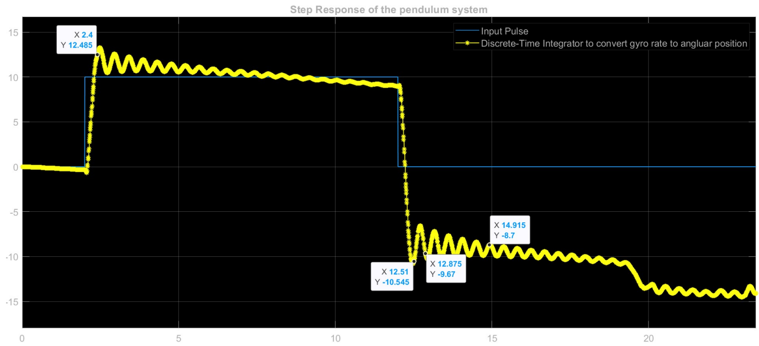

Figure 1: Pulse response of the pendulum

From Figure 1 seen below, the natural frequency of the system was found to be $\omega_n = 2.01 \times 2\pi = 12.65 rad/s$. Consequently, the value k was found to be:

$$k = \omega_n^2 = 12.65^2 = 158$$

Using the steady state angle after the step is applied, the gain of the system can be found as:

$$c = \frac{\theta_{ss}}{V} \times k = \frac{12.5}{10} \times 158 = 198$$

Finally, the parameter b was calculated by finding the approximate setting time of 5τ, where $\zeta\omega_n = \tau$:

$$b = 2\zeta\omega_n = 2 \times \frac{5}{1.79} = 5.6$$

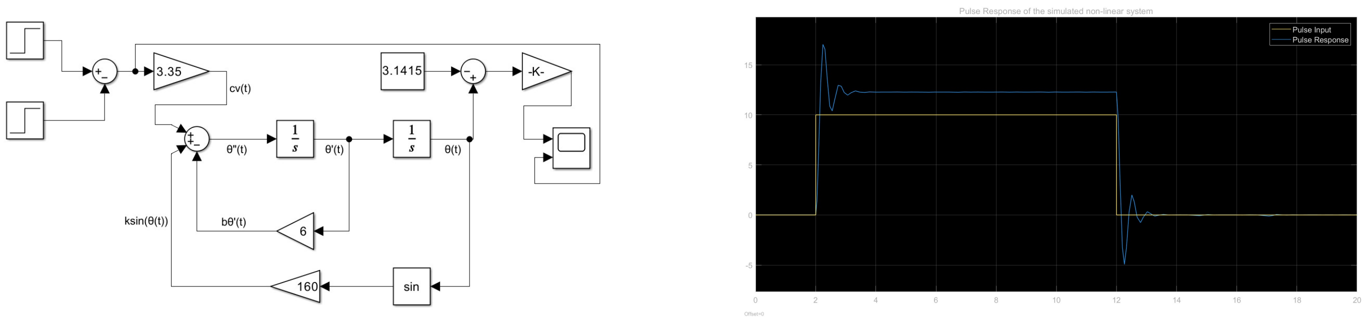

(a) Non-linear simulink model of the system

(b) Pulse response of the non-linear simulation

Figure 2: Non-linear simulink model and the corresponding pulse response simulation

By further tuning for the non-linear nature of the system by systematically incrementing individual parameters, numbers that better match the response of the physical experiment can be found, thus we can form a more accurate plant model as seen in Figure 2b. The resulting plant transfer function is approximately:

$$G(s) = \frac{192}{s^2 + 6s + 160}$$

3 Phase-Lead Controller Design

The selection of a crossover frequency ($\omega_c = 30$ rad/s) represents a strategic compromise in controller design. While increasing ω_c enhances system bandwidth, improves reference tracking, and speeds up transient response, it is constrained by the excitation of unmodeled dynamics, the risk of actuator saturation due to excessive controller gain as well as given upper bound of the complementary sensitivity function bandwidth. Consequently, $\omega_c = 30$ rad/s was chosen as it balances effective disturbance rejection without exceeding the physical capacity of the LEGO EV3 hardware.

While a higher phase margin serves as a crucial ”shock absorber” that increases the damping ratio (ζ) to eliminate mechanical wobble and buffer against physical hardware delays, demanding excessive phase boost forces the compensator’s zero, Z_{lead}, toward the origin and its pole, P_{lead}, deep into the left-half plane. This extreme pole-zero separation traps a closed-loop pole near the imaginary axis due to the phase-lead pole near the origin, resulting in a long settling time, while the distant pole amplifies high-frequency sensor noise. As an act of balance, the phase margin is chosen to be 50 degrees.

With these two design parameters chosen, a Phase-Lead Controller takes the form of:

$$C(s) = \frac{K(\tau_z s + 1)}{(\tau_p s + 1)}$$

The maximum phase boost (ϕ) occurs at the geometric mean of the pole and zero

$$\omega_c = \frac{1}{\sqrt{\tau_z \tau_p}} \quad \text{and} \quad \phi = \arcsin \quad \frac{\tau_z - \tau_p}{\tau_z + \tau_p}$$

By rearranging the phase equation and substitution of ω_c gives

$$\frac{\tau_z - \tau_p}{\tau_z + \tau_p} = \sin(\phi) \quad \text{and} \quad \tau_p = \tau_z \frac{1 - \sin(\phi)}{1 + \sin(\phi)}$$

$$\Rightarrow \tau_p = \frac{1}{\omega_c} \cdot \sqrt{\frac{1 - \sin(\phi)}{\sin(\phi) + 1}} \quad \text{and} \quad \tau_z = \frac{1}{\omega_c^2 \tau_p}$$

From Figure 3a, the plant has a phase of 170 .36° at $\omega_c = 30$ rad/s

$$\Rightarrow \phi_m = \text{PM}_{target} - (180^\circ + \angle G(j\omega_c)) = 50 - (180^\circ + 170.36^\circ) = 40.36^\circ$$

$$\Rightarrow \tau_z = \frac{1}{12.32} \approx 0.0812 \text{ s}, \quad \tau_p = \frac{1}{73.08} \approx 0.0137 \text{ s}$$

To place the crossover frequency at exactly where we designed, K was calculated to be:

$$K = \frac{1}{|G(j30)C(j30)|} = 2.2988$$

$$\Rightarrow C(s) = \frac{2.2988(0.0812s + 1)}{(0.0137s + 1)} = \frac{13.6412s + 168.00}{s + 73.08}$$

The algorithmic design process successfully met the phase margin and crossover frequency specifications, as demonstrated in Figure 3b. To verify closed-loop stability, Figure 4a plots the root locus of the open-loop system, with the calculated closed-loop poles highlighted in green. Because all closed-loop poles reside strictly in the left-half plane (LHP), system stability is confirmed. The dominant pole is located at $s = -9.09$, corresponding to a dominant time constant of 0.11 s. Note that one high-frequency open-loop pole at $s = -73.08$ falls outside the visible axis limits of the figure. Finally, the bandwidth of the complementary sensitivity transfer function was evaluated at 28 rad/s, successfully satisfying the 50 rad/s upper-bound specification.

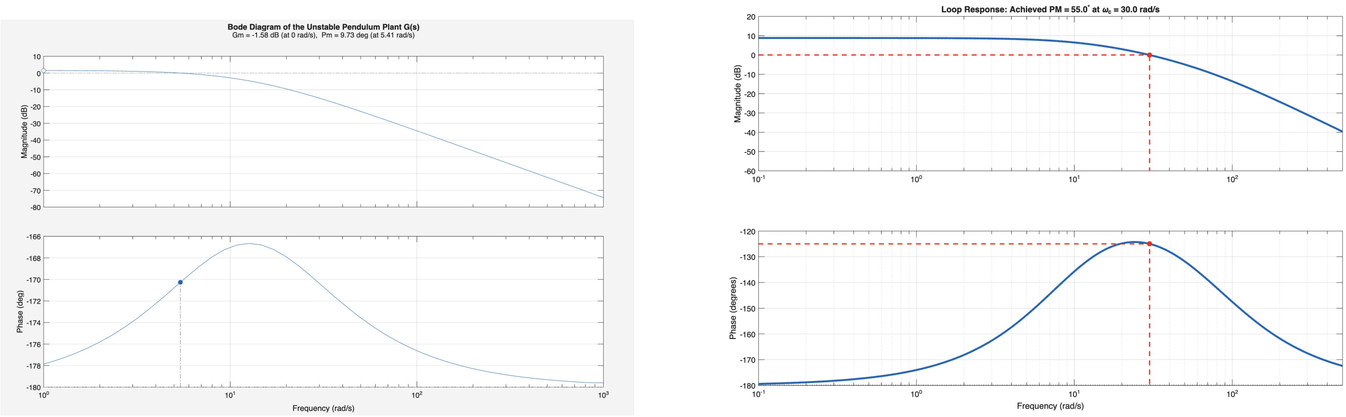

(a) Plant model Bode and Phase Plots

(b) Open loop System Bode and Phase Plots

Figure 3: Bode plots of plant model and open loop system

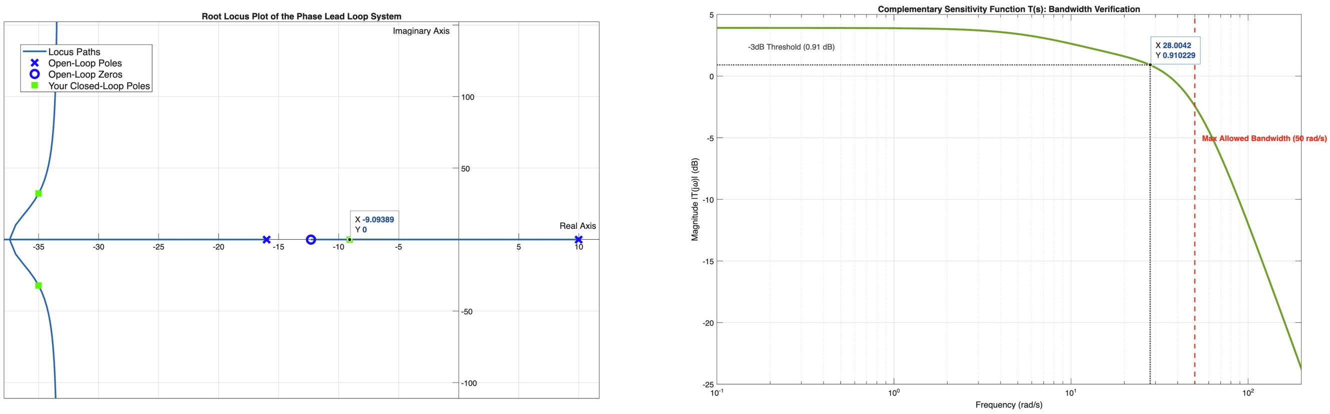

(a) Root locus plot of open loop system

(b) Magnitude Plot of T(s)

Figure 4: Root locus plot of open loop system and magnitude plot of T(s)

4 Implementation and Testing

4.1 Simulation Testing

Prior to physical implementation, the designed controller was validated in simulation using the derived plant model, controller and then adding the necessary disturbances, incorporating the pendulum dynamics. In terms of adequate disturbance rejection, the simulation results in figure 5a show that while the robot is stationary and an impulse disturbance is applied via a square wave, the controller drives the pendulum motor to correct the angular position of the pendulum to near zero shortly after each impulse, demonstrating effective disturbance rejection. Likewise in figure 5b, when the robot is steering, represented by a triangle wave, it can be seen once again that despite the angle deviation, the robot is capable of reorentating the pendulum to the reference angle quickly and robustly. Hence, through simulation, it stands to reason that the controller is capable of rejecting both impulse disturbances as well as continuous base disturbances.

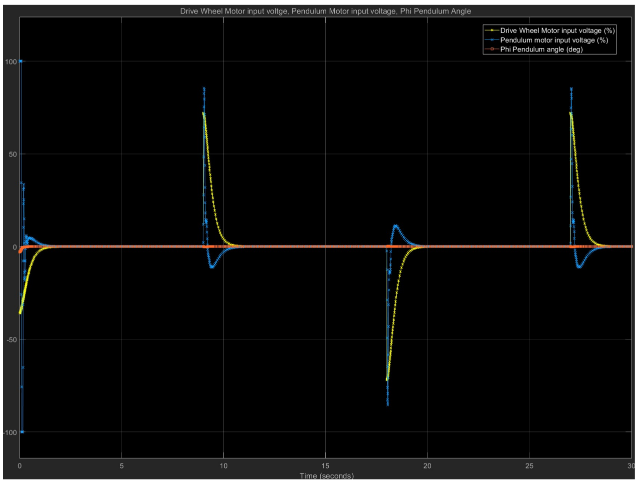

(a) Simulated system impulse disturbance response

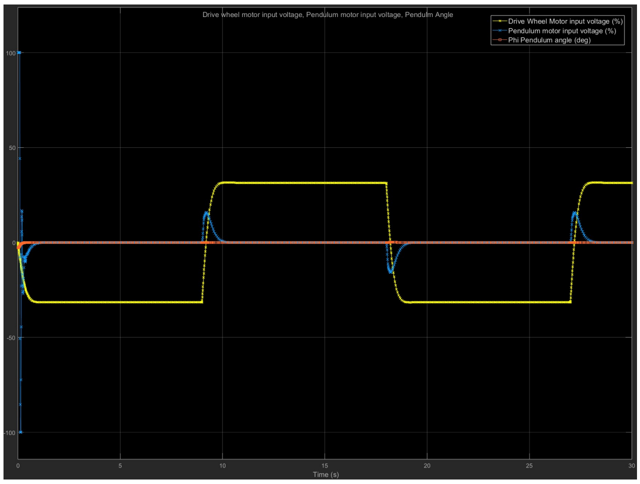

(b) Simulated system constant disturbance response

Figure 5: Simulated system responses to disturbance

4.2 Controller Discretisation

The continuous time controller $C(s)$ was discretised for implementation on the EV3 robot. A sample period of $T_s = 0.005$ seconds was selected to ensure it was sufficiently small relative to the closed loop bandwidth. The Tustin method was used and implemented via MATLAB to preserve frequency domain characteristics near the crossover frequency. The resulting discrete time transfer function $C(z)$ was implemented in the EV3 Simulink block diagram using the 'Discrete Transfer Fcn' and gain blocks.

4.3 Experimental Validation

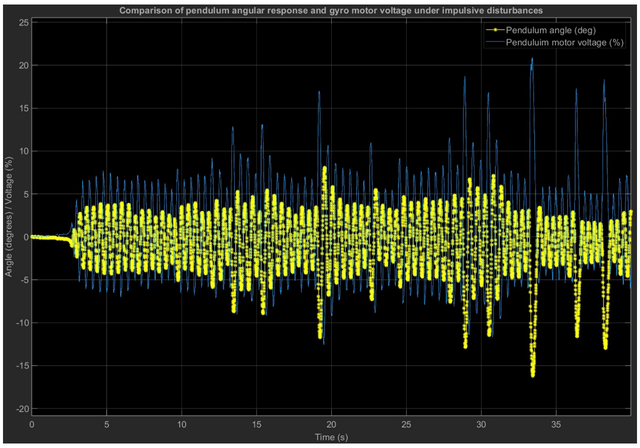

(a) Experimental system impulse disturbance response

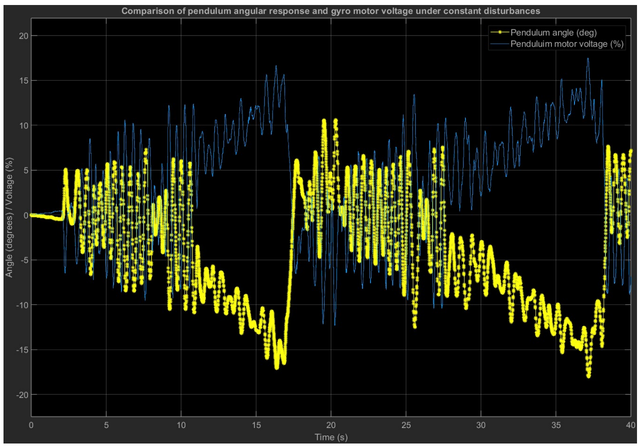

(b) Experimental system constant disturbance response

Figure 6: Experimental system responses to disturbance

The control system was implemented and tested on the LEGO EV3 robot using Simulink External Simulations where gyro sensor data from the pendulum can be communicated with Simulink for monitoring and analysis to meet key specifications. With the pendulum starting near the upright position, the controller maintained balance for an extended period, demonstrating closed loop stability. When a manual impulse was applied to the top of the stationary pendulum, figure 6a shows that the pendulum returns to the 0 degree reference angle, confirming impulse disturbance rejection. A similar test with the triangle wave steering maneuver, as seen in figure 6b, showed recovery to the upright position despite an even greater deviation from the reference angle, confirming robustness to constant disturbance. Despite the oscillatory behaviour about 0 degrees, which will be discussed shortly, figure 6a shows that under no disturbance, the measured angle does not deviate greater than 5 degrees either side of the reference angle. The constant disturbance produced much larger deviations than the impulse tests, yet in both cases the pendulum always returned to 0 degrees which is consistent with simulation predictions. This therefore serves to show that the system is robust, meeting disturbance rejection objectives as it is able to regulate and reject both applied impulse and constant disturbances.

It is worth noting that the pendulum angle and pendulum motor traces of figure 6 are reflective of eachother about the x-axis. This is because the controller generates a control action that acts in the direction required to oppose the pendulum's displacement from the upright position. Hence, when the pendulum tilts in the positive direction, a negative motor voltage is commanded to drive the pendulum back to the upright position to restore balance. Conversely, when the pendulum tilts in the negative direction, a positive motor voltage is applied. As a result, the motor voltage is approximately proportional to the negative pendulum angle, causing the two signals to appear as reflections of one another about the x-axis.

With that being said, it is clear when comparing the simulation to the experimental results that there are a few discrepancies, namely an increase in oscillatory behaviour in conjunction with a slower disturbance rejection response. There are many reasons for this behaviour such as unmodeled nonlinearities like friction, motor deadzones, gyro drift, battery voltage levels, or other parameter uncertainties in b, k, and c of the plant model. The oscillations stem from the gain of the controller being too large. However, this was a necessary tradeoff since in practice, a smaller gain would reduce the effectiveness of the disturbance rejection, often resulting in the EV3 robot falling to one side. Possible improvements that may incorporate some of these assumptions are explored in the following section.

While the phase lead controller significantly improved the transient response and stability margins of the system, it has a non-zero steady state error which may remain when tracking step references or rejecting constant disturbances as shown in the results. These characteristics are to be expected since by the internal model principle, perfect asymptotic disturbance rejection requires the loop to contain a model of the disturbance generator. Since the designed controller contains no integrator, there is no internal model of the DC component of the base disturbance arising from the robot steering, and a small residual steady state deflection in the pendulum angle is therefore expected and observed. Regardless of these limitations, it can be said that the controller implemented meets specifications, capable of balancing the pendulum in the upright position while disturbed by both a sudden impulse and constant disturbance from steering.

5 Conclusion

A nonlinear pendulum model was derived and linearised about the upright equilibrium, with parameters identified by matching the transfer function response to experimental step data collected using MATLAB/Simulink and the physical EV3 platform.

A Phase-Lead controller was designed and validated through both simulation and hardware testing. Results demonstrated that the controller successfully maintained the pendulum in the upright position under nominal conditions, and exhibited adequate robustness and correction to external disturbances including manual impulses applied to the pendulum arm and constant disturbances induced by robot steering. Both theory and experiment confirmed that the three performance specifications (a phase margin of at least 40 degrees, effective disturbance rejection, and a complimentary bandwidth not exceeding 50 rad/s) were satisfied.

Possible improvements include incorporating integral action, ultimately satisfying the internal model principle, whereby the integrator introduces a pole at the origin, providing the internal model required for better tracking of constant reference signals and better rejection of constant disturbances. This modification would improve steady state accuracy while retaining the transient performance benefits. Careful tuning would be necessary to balance the improved steady state performance against potential reductions in phase margin and stability. A more accurate model accounting for motor nonlinearities, joint friction, and battery voltage variation could also improve simulation fidelity and controller performance. Overall, the project reinforced the critical role of feedback control in stabilising inherently unstable systems and highlighted the practical challenges of bridging model based design with physical hardware implementation.

A Contribution Statements

James Teng	System data collection, Simulink Controller Design, Lego Kit Controller Testing
Tuong Bao Nguyen	Introduction, Simulation, Testing and Implementation, Conclusion
Ethan Ng	System Modeling

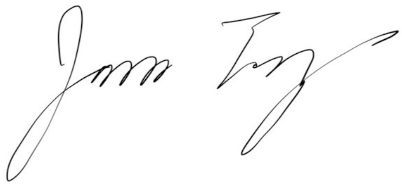

(a) James Teng

(b) Tuong Bao Nguyen

(c) Ethan Ng